Available online at www.sciencedirect.com
SCIENCE DIRECT®
Nuclear Instruments and Methods in Physics Research A 551 (2005) 330–338
NUCLEAR INSTRUMENTS & METHODS IN PHYSICS RESEARCH Section A
www.elsevier.com/locate/nima

A high-efficiency compact setup to study evaporation residues formed in reactions induced by low-intensity radioactive ion beams ☆

D. Shapira[a,*], J.F. Liang[a], C.J. Gross[a], R.L. Varner[a], H. Amro[b], C. Harlin[c], J.J. Kolata[b], S. Novotny[d,e]

[a] *Oak Ridge National Laboratory, Physics Division, Oak Ridge, TN 37831, USA*
[b] *Physics Department, University of Notre Dame, Notre Dame, IN 46556-5670, USA*
[c] *Department of Physics, University of Surrey, Guildford GU2 7XH, UK*
[d] *Oak Ridge National Laboratory, Oak Ridge, TN 37831, USA*
[e] *University of Heidelberg, Heidelberg, Germany*

Received 10 March 2005; received in revised form 27 March 2005; accepted 27 May 2005
Available online 22 July 2005

Abstract

A setup for measuring cross-sections of evaporation residues produced in the collision of two heavy ions is described. The system, which detects all reaction products in a narrow angular range around the beam direction, is designed to work best with low-intensity beams ($\leqslant 10^5$ ions/s) and can be highly efficient for reactions studied in inverse kinematic conditions, i.e., heavy-mass beam on lighter-mass targets. The system as presented here has been optimized to study evaporation residues from reactions induced by radioactive ion beams with charges near $Z\sim 50$ and energies near 4 MeV/nucleon. Continuous sampling of the beam velocity, energy loss and position allow for the measurement of accurate evaporation residue cross-sections also in situations where the beam contains a mixture nuclides.

PACS: 25.70Jj; 24.10Eq; 25.60

Keywords: Fusion evaporation; Time of flight; Ionization chamber; Position sensitive detectors; Timing detector

1. Introduction

The fusion of heavy ions at sub-barrier energies has been the subject of intense study since it was discovered that the magnitude of these fusion cross-sections far exceeds the values expected from

☆ Research sponsored by the Office of Science, US Department of Energy, under contract DE-AC05-00OR22725 with UT-Battelle, LLC. H.A. and J.J.K. are supported by NSF Grant PHY02-44989.
*Corresponding author. Tel.: +1 865 572 2648; fax: +1 865 574 1268.
E-mail address: shapirad@ornl.gov (D. Shapira).

0168-9002/$ - see front matter © 2005 Elsevier B.V. All rights reserved.
doi:10.1016/j.nima.2005.05.079

quantum mechanical penetration of a one-dimensional Coulomb barrier [1–3] and the realization that the enhancement in cross-section shows strong dependence on the structure of the colliding nuclei. It is expected that compound nucleus survival probability increases with the neutron number available for the compound system and some data suggested that an excess of neutrons in the colliding partners will result in large enhancement of fusion cross-sections [4]. Other studies suggest that the preponderance of open neutron transfer channels would bring about large enhancement of these cross-sections [5–7]. The availability of accelerated beams of unstable nuclei at HRIBF as well as other facilities [8,9] presents the possibility of extending studies of sub-barrier fusion to systems with large number of neutrons or protons. These studies may well lead to a better understanding of the role that neutron excess plays in enhancing sub-barrier fusion and may pave the way for using neutron-rich radioactive nuclei in continued efforts to synthesize heavier nuclei [10].

Great opportunities are usually accompanied by new challenges. The intensities of radioactive beams diminish farther from stability, and often the beams available are mixtures of nuclides (depending on the facility and production methods). While improvements to the purity and intensity of radioactive beams are expected at future facilities, both may remain low for beams closer to the neutron drip line. Experiments will have to employ methods to mitigate the effects of beam impurity and low beam intensity.

In the study of rare processes, it is usually necessary to physically separate the beam from the desired reaction products. To that end, velocity filters, mass separators or other means of magnetic or electrostatic separation are commonly used [11]. Most devices present a tradeoff between clean and precise separation and spectrometer acceptance. Gas-filled magnetic separators, first introduced by Cohen and Fulmer [12], are most efficient but less selective and are used in the study of evaporation residues [13]. At HRIBF, we have commissioned a gas-filled separator that is suitable for separating evaporation residues from reactions induced by lighter fission products, derived from p + U fission (As, Ge, etc.) [8], on medium mass targets [14]. This system, however, could not be used for similar studies with the heavier fission products (Sn, Te, etc.) because the Enge Split Pole Spectrograph (ESPS) does not have sufficient bending power (K) to deflect the residues to the focal plane. This is particularly true with inverse kinematic reaction conditions and the low average charge states produced in a dilute gas. We, therefore, devised a system with which we could study evaporation residues from reactions induced by beam with Z near 50 and energies near 4 MeV/nucleon. This article describes the system and lists its capabilities, limitations and some possible improvements.

2. CSSER—Compact System for Studies of Evaporation Residues

A block diagram of the system is shown in Fig. 1. Two timing detectors are placed upstream from the target and used for determining beam properties and a third timing detector, placed downstream from the target, provides a time gate to separate particles that move appreciably slower than the beam (e.g., evaporation residues).

The two detectors used for beam timing are described in [15]. For completeness sake we show a diagram of the timing detector in Fig. 2 with a summary of capabilities listed in the figure caption. More details of the detector's performance and capabilities appear elsewhere [16] and in the original article [15].

As already mentioned, the two timing detectors (1st and 2nd in Fig. 1) are used to gate on beam velocity. In our experiments at HRIBF, they also provide a beam trigger that is scaled down and combined with other event triggers. This, as will be shown later, facilitates normalization of measured cross-section data.

Downstream from the target are two detectors that are used to identify and isolate yields associated with evaporation residues in the reaction. About 20 cm downstream from the target we have a third timing detector that is very similar to the other two upstream detectors, but instead of a simple metal anode, it has a resistive layer. The charges collected at four corners of this resistive

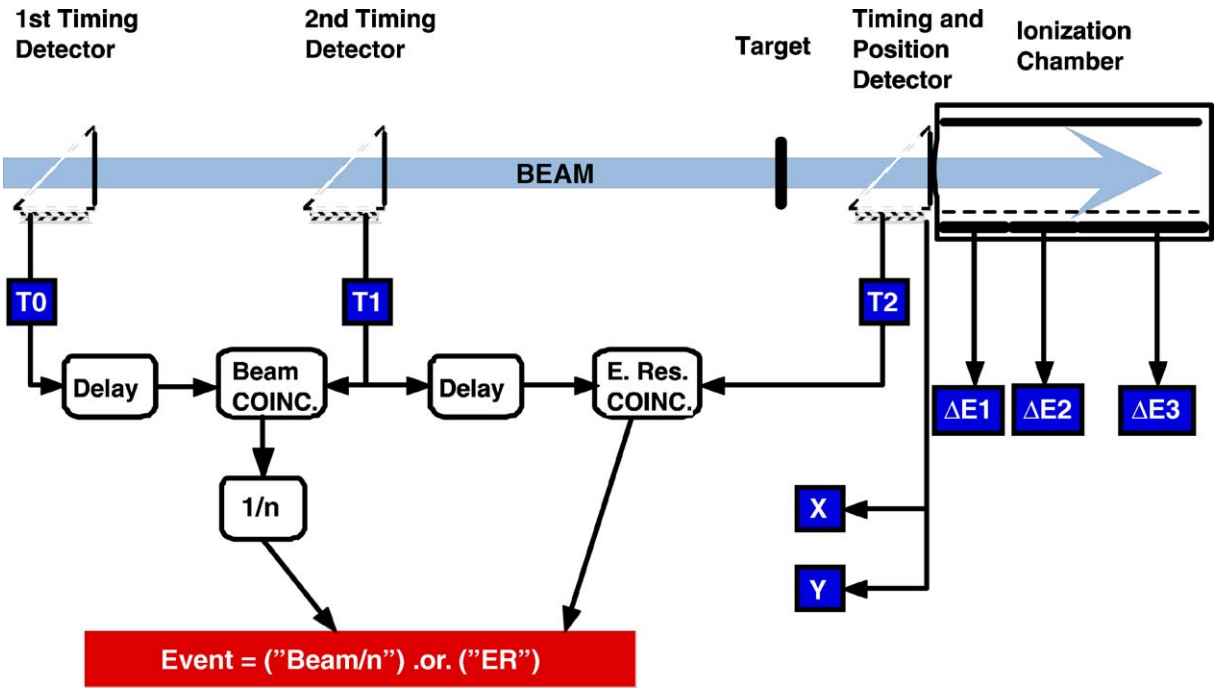

Fig. 1. A block diagram showing the main elements of our detection system. The dark boxes represent the different signals (parameters) that are recorded every time a valid event occurred. A valid event could be either a particle slower than the beam or a down scaled sample of the beam.

layer are used to calculate the positions at which the amplified electron current exits the MCP plates. As can be seen from the electron trajectories displayed in Fig. 2, the position at the exit of the MCP plate will reflect, with some unavoidable spread, the position at which the charged particle (beam or reaction product) hit the foil. We have not done an exhaustive study of the position resolution of this device but have shown in previous work [17] that we can anticipate about 2 mm FWHM with the accelerating voltages shown in Fig. 2. This may not be sufficient for ray tracing but allows us to examine the beam profile and verify that the beam is well centered.

The final element of our setup is an ionization chamber. As shown in Fig. 1, the ionization chamber window (opening 2.5 cm diameter) is placed very close to the third timing detector. The angular acceptance of this detector arrangement is a cone of about 3.5° (half-angle) around the direction of the beam emanating from the center of target. The ionization chamber is 30 cm deep and the detector's height, defined by the cathode to Frisch grid distance of 7 cm, allows for containment of the trajectories for all reaction products emanating from the target's center. The first two anodes are 7.5 cm long and the third anode is 15 cm long and measures the residual energy of stopped particles. We use CF_4 gas which combines good stopping capabilities and fast electron mobility. This choice of gas along with the compact dimensions of this detector minimize electron drift times in the ionization chamber. At 1 V/cm/Torr, the ionization chamber can therefore operate at rates higher than 50 kHz without significant deterioration to signals.

The system shown in Fig. 1 provides a fast trigger from two event types. The first is a scaled down coincidence between the first and second timing detector, with delay time adjusted to trigger on particles having beam velocity. These beam events are combined with coincidences between the second and third timing detectors with delays adjusted to trigger on particles that move more

slowly than the beam. This condition is not exclusive for evaporation residues, yet we label the events in this gate as "evaporation residue"

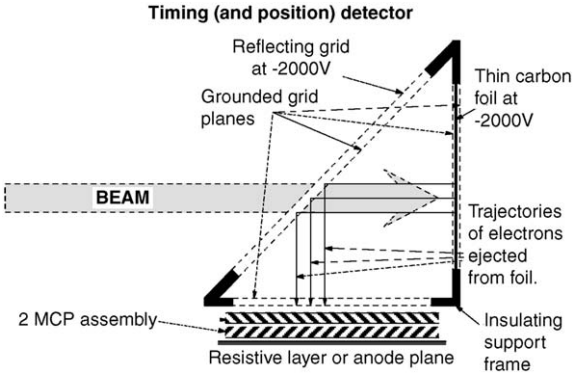

Fig. 2. Diagram of the timing detectors. The detected beam particles pass through a thin foil and cause the emission of electrons from the foil surface. These electrons are accelerated away from the foil which is biased to −2000 V by the grounded grid. The electrons are then deflected toward an MCP detector by the slanted electrostatic mirror. The MCP detector provides for fast amplification of the electron signal. With the accelerating voltages that are shown in the figure, timing resolution of 100 ps (FWHM) was achieved and count rates in excess of 1 MHz were accommodated with no noticeable degradation in time resolution.

events (see Fig. 1). The combined master event results in a trigger rate of less than 1 kHz, no loss of events of interest (evaporation residues) and minimal computer dead time. For each event trigger, the acquisition system reads the time of flight (time to amplitude converter output) between the different timing detector pairs, the energy and energy loss signals from the ionization chamber and the position signals from the third timing detector's resistive anode. The position signals are used to monitor the position (in a plane perpendicular to the beam axis) of all particles entering the ionization chamber during the experiment. When gated on scaled down beam events, this position spectrum provides a continuous sample of the beam profile and allows the experimenter to detect any shifts in beam position. This information is crucial for monitoring the detection efficiency of evaporation residues, especially when the projectile mass is close to the target mass.

Fig. 3 shows two DE1 vs DE2 maps obtained with the ionization chamber running with the same gas pressure and voltages. On the left, we show signals from collisions of 560 MeV ^{124}Sn with ^{64}Ni for the combination of evaporation

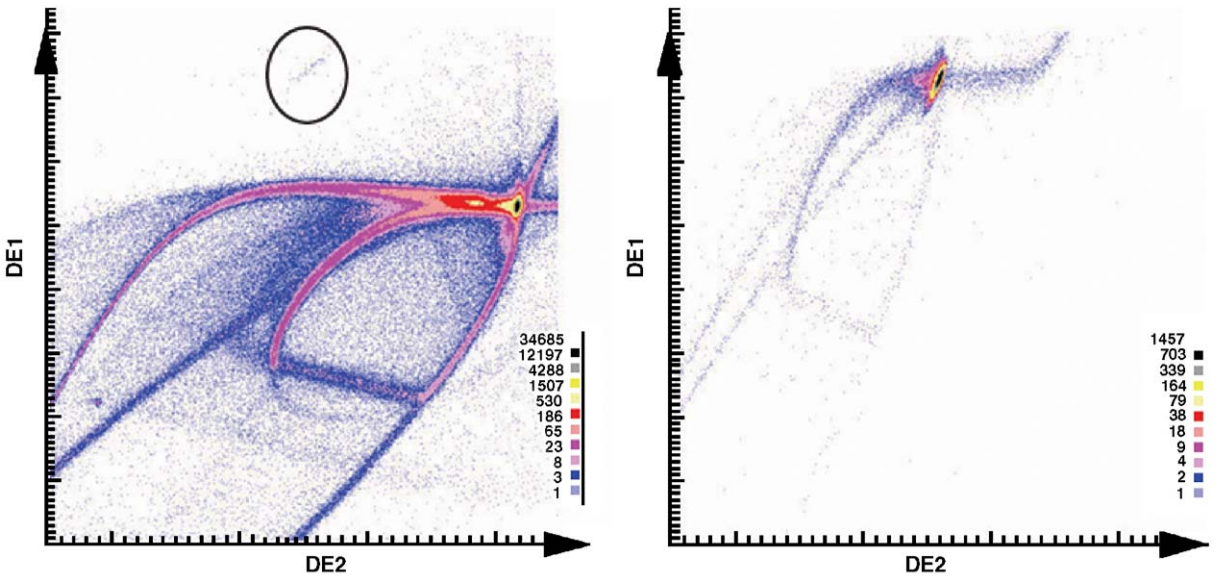

Fig. 3. Two-dimensional plots of DE1 vs DE2 showing identified evaporation residues in ^{124}Sn + ^{64}Ni and for a ^{197}Au beam at energies matching the evaporation residues.

residue events and beam events scaled down by 200 (ER + Beam/200). We have circled the yield that we identified, based on a rough energy calibration, as the group of evaporation residues (i.e., mass near 190 and charge near 78). On the right side is the DE1 vs DE2 spectrum of a 375 MeV gold beam (without target) stopped in the ionization chamber. This comparison assures us that we have not mis-identified the evaporation residues. Integrating the yield of the group circled in the left panel and counting the number of beam particles that passed through the target is all we need to determine the evaporation residue cross-sections for a given (pure) target and beam.

For heavy systems $A_{CN} \geqslant 100$, at low bombarding energies, the compound nucleus (CN) emits mostly neutrons and occasionally some protons. This is especially true for neutron-rich systems. As a result, the compound nucleus does not recoil to large angles and stays close to the beam axis. Under these circumstances, the efficiency of detecting the evaporation residues with our system is quite high. This is especially true for reactions where the mass of the beam is greater than the mass of the target. In the case of 560 MeV, ^{124}Sn on ^{64}Ni Monte Carlo simulations (using events from PACE2 [18] and allowing for multiple scattering in the target) show our system to be 96% efficient in detecting evaporation residues. Small shifts of 1–2 mm in beam position hardly affect this efficiency and larger deviations can be easily spotted since we monitor the beam position continuously.

Fig. 4 shows the beam spots obtained in two runs taken with the same beam but with the third timing detector displaced by 4 mm. The plot on the left shows the beam spot when the detector was positioned at a height of 29 mm and the one on the right shows the beam spot with the detector positioned at a height of 33 mm. Shifts of 4 mm in beam centroid position could result in some loss of efficiency for capturing residues. As we mentioned before, such changes in efficiency can be corrected by simulating the detector's response to evaporation residues using the event files from an evaporation code (PACE2 [18]). However, since these spectra are monitored during the experiment, it is easier to re-tune the beam to the correct position.

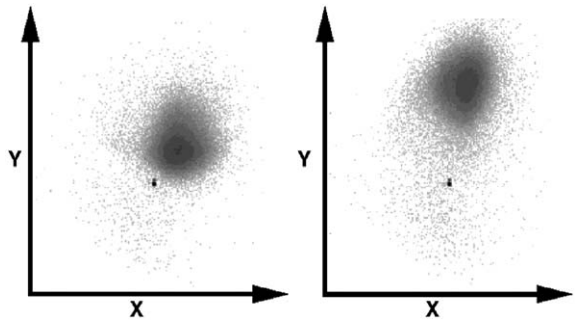

Fig. 4. Beam profiles with detector positioned at (left) 29 mm height (the nominal position) and (right) 33 mm height.

Often beams at radioactive beam facilities contain mixtures of nuclides. The system described here allows for the measurement of cross-section for evaporation residue production in situations where mixed beams are present. A case in point is the measurement of evaporation residue cross-sections for ^{134}Sn + ^{64}Ni [19]. The ^{134}Sn beam at HRIBF contains several contaminants mostly ^{134}Te (about 50–70%) and small percentages of ^{134}Sb and ^{134}Ba [8]. Cross-sections for evaporation residue formation at sub-barrier energies tend to decrease rapidly as the ratio between the bombarding energy and the Coulomb barrier decreases. Therefore, the contamination from beams with higher charge (Z) would pose less of a problem especially if they are of small relative intensity. The ^{134}Te contaminant in the beam, though, poses a problem because it is substantial and at energies near and above the barrier, there is no telling whether residues are formed from ^{134}Te + ^{64}Ni or from ^{134}Sn + ^{64}Ni. In order to extract the ^{134}Sn cross-sections, we first measured data with ^{134}Te + ^{64}Ni and then measured with the mixed beam. Since our detectors sample the beam continuously we obtain for each run, the number of ^{134}Te and ^{134}Sn beam particles incident on the target. Fig. 5 shows a DE1 vs Esum (= DE1 + DE2 + DE2) spectrum gated for beam events only. This spectrum clearly shows that we can separately integrate the number of Sn and Te isobars in the beam. The number of incident ^{134}Te and ^{134}Sn beam particles, combined with the cross-sections for evaporation residue formation in ^{134}Te + ^{64}Ni,

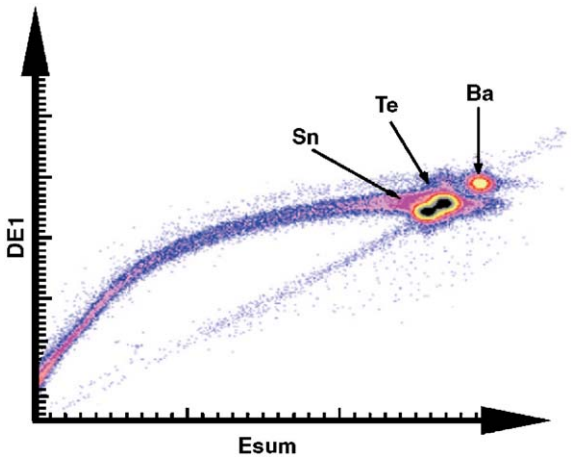

Fig. 5. Two-dimensional plot of DE1 vs Esum for beam events only in a $^{134}Sn + ^{64}Ni$ experiment revealing the isobaric contamination of the beam.

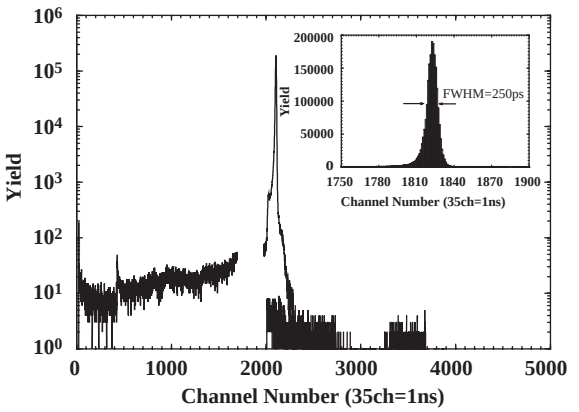

Fig. 6. Timing spectrum for the first two timing detectors—for beam events. The inset shows an expanded portion of the spectrum displayed on a linear scale showing timing resolution of about 250 ps.

allow us to extract the cross-sections for evaporation residue formation in $^{134}Sn + ^{64}Ni$.

3. Capabilities and limitations

Our system has some unique features that must be dealt with:

- The beam is often a mixture of nuclides.
- Since the beam enters all the detectors, a high rate of random background counts results.
- The low beam intensity necessitates the use of thick targets.

In this section, we provide some details of how we mitigate these problems and extract useful information from the data.

3.1. Beam timing

A spectrum of the timing between detectors T1 and T2 taken with 450 MeV ^{124}Sn beam is shown in Fig. 6. Typical beam kinetic energies in these experiments are around 4 MeV/A resulting in flight times around 36 ns over a distance of 1 m. To separate nuclides of mass 130 and 131 would then require timing resolution near 200 ps, which is achievable with these detectors. At higher velocities, such as are available at fragmentation facilities larger distances between the two beam timing detectors T1 and T2 (see Fig. 1) would be required. At HRIBF, the only contaminants in the beam that concerns us are isobars which are very close in mass and inseparable with the available time-of-flight resolution. As we have shown in the previous section, we dealt with this problem by sampling the beam in the ionization chamber. In a separate publication [20] we show that by combining energy loss and time-of-flight measurements, isobars can be separated a with similar arrangement of timing detectors and absorbers placed in the beam's path.

3.2. Background suppression

A major problem with an approach that does not physically remove the beam from the detector system is the presence of a large background of random counts that could mask rare events of interest. This can be mitigated by requiring several independent gating conditions, but this will ultimately place a lower limit on the cross-section of detectable events. A typical case presented below shows how we estimate the capability of the system to isolate evaporation residues when the detectors are exposed to the full beam current.

In an experiment to study sub-barrier evaporation residue yield from $^{132}Sn + {}^{64}Ni$ we had the following conditions [21,22]:

- Beam intensity 20,000 ion/s.
- Target thickness 1 mg/cm^2.
- Evaporation residue cross-section 1 mb.

The expected rate of evaporation residue production under these circumstances is about 2×10^{-3} counts/s. One can now estimate the random rates for any of the signals used to identify the evaporation residues. These depend mostly on the resolving time of the signal selected for processing. The ADC gates for the ionization chamber signals were about 1 μs wide. Timing gate requirements are set by the observed spread in residue velocities which is about 3 ns. The random rates for each signal are therefore:

- DE1 or DE2 within a time bin of 1 μs,
  $2 \times 2 \times 10^4 \times 2 \times 10^4 \times 10^{-6} = 8 \times 10^2$ counts/s.
- DE1 and DE2 within a time bin of 1 μs,
  $2 \times 2 \times 10^4 \times 8 \times 10^2 \times 10^{-6} = 32$ counts/s.
- Time-of-flight cut on DE1 and DE2 within a 3 ns time bin,
  $2 \times 2 \times 10^4 \times 32 \times 3 \times 10^{-9} \sim 4 \times 10^{-3}$ counts/s.

With an expected event rate of 2×10^{-3} counts/s we see that we are near the lower limit of cross-sections that can be measured with this method. We must employ a method where the evaporation residue yield can be identified and isolated as in Fig. 3. This cannot be achieved when regions of the DE1 vs DE2 plot have the same number of random counts as the number of expected evaporation residue events. It is clear that at higher beam rates random counts will be overwhelming. However, this can be mitigated somewhat by applying tighter timing gates. Note that a rate of 0.002 events/s requires a running time of 16 h to acquire more than 100 events. The only way to improve on these prospects is to allow for faster time gates on the ADCs reading the ionization chamber signals. Since there is an inherent jitter in the DE arrival time due to the spread in electron drift times it would be hard to get significantly below 300 ns. In the following section, we will show how tightening the time gates allows one to extract lower residue cross-sections.

3.2.1. *Low cross-section*

Fig. 7 shows an excitation function for evaporation residue cross-sections for the reaction $^{124}Sn + {}^{64}Ni$. As can be seen, the data we measured are in good agreement with the data obtained previously by Freeman et al. [23].

Fig. 8 shows four DE1 vs DE2 plots of ionization chamber signals for different cases. Unlike the case shown in Fig. 3, the data in Fig. 8A, taken for the case of $^{124}Sn + {}^{64}Ni$ at 470 MeV do not show any clear indication as to the location of the evaporation residue group. The arrow points at the cluster of events where we expect the evaporation residues to appear. However, applying a 3.5 ns wide time gate on T3–T2 around the time region where evaporation residues are expected results in the spectrum shown in Fig. 8B. The cluster of evaporation residue events stands out clearly with very little background. This was the situation for data corresponding to cross-sections around 20 mb (an event rate of about 0.04 counts/s). At lower energies, applying the same 3.5 ns wide gate is not sufficient as shown in Fig. 8C. These are data taken at 450 MeV bombarding energy, the expected location of residues in the DE1 vs DE2 plot is indicated but the yield does not stand out. The situation can be

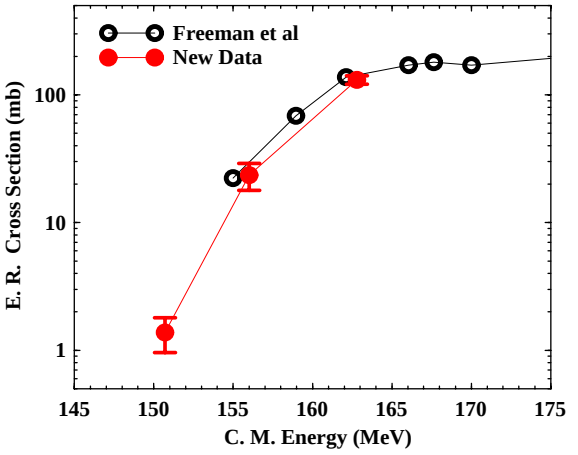

Fig. 7. Evaporation residue cross-section for $^{124}Sn + {}^{64}Ni$. The open circles are data by Freeman et al. [23].

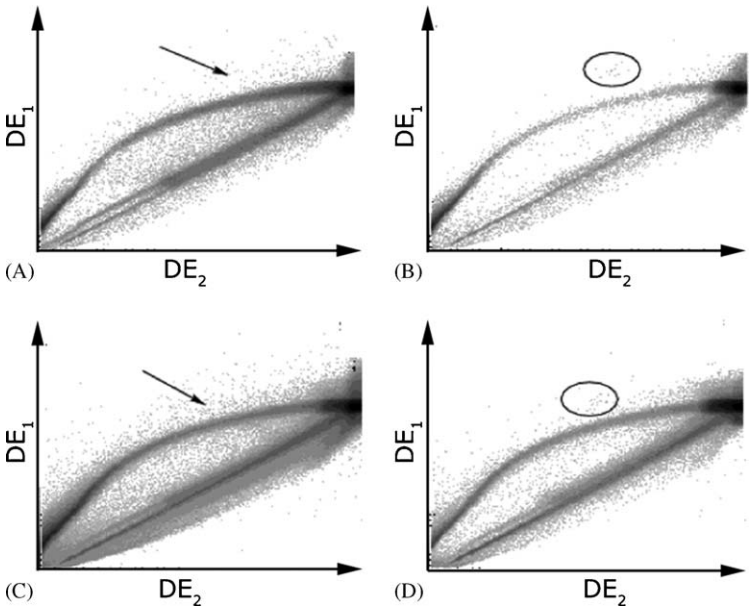

Fig. 8. DE1 vs DE2 spectra used to select evaporation residues. See text for detailed explanations.

improved by applying narrower time gates. Fig. 8D shows the 450 MeV data with a 0.3 ns time gate. One can now identify the cluster of evaporation residue events. It is apparent from Fig. 8D that there is still some background that should be subtracted. In order to determine this background we apply successive, equally spaced, gates of 0.54 ns width over the time region where evaporation residues are expected and plot the integrated yield as a function of delay time. Fig. 9 displays several yield curves extracted with the same procedure but with different evaporation residue gates drawn around the same group in Fig. 8D. As can be seen from Fig. 9 the background can be subtracted quite reliably.

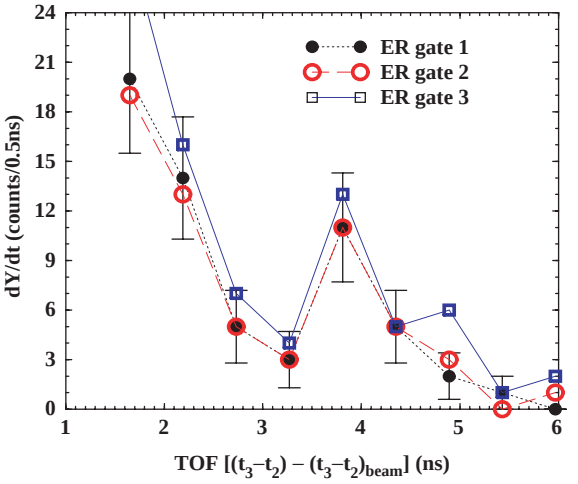

Fig. 9. Differential of evaporation residue yield taken in 0.5 ns wide time bins plotted as a function of delay time relative to beam's flight time between timing detectors 2 and 3. The errors are due to counting statistics. The gate labeled ER gate 3 is shown in Fig. 8D, the other two gates are tighter gates drawn around the same group.

3.3. Thick target

In experiments involving low-intensity radioactive beams one is often forced to use thick targets. Beam energy loss in the target was substantial in our case (about 40 MeV) and was determined by direct measurement of beam energy in the ionization chamber. At sub-barrier energies the evaporation residue cross-section decreases exponentially with beam energy. As a result, the cross-section near the entrance of the target has more weight than the cross-section near the exit of the target. It is crucial, therefore, to obtain the form of the excitation function and perform a

proper weighted average to determine the reaction energy associated with the measured cross-section.

An iteration method was used to determine the reaction energy for the thick target measurement. First, we took the measured cross-sections and the beam energy at a depth half-way into the target and fitted these points with a three-parameter logarithmic function

$$\sigma(E) = (\alpha^2\beta/2E)\ln\{1 + \exp[2\pi(E-\gamma)/\beta]\}$$

where $\sigma(E)$ and E are the measured cross-section and input energy, respectively, and α, β, and γ are three fitting parameters.[1] Once the three parameters were found, the functional form was used to calculate the cross-section weighted energy for each data point using

$$\overline{E} = \frac{\int E\sigma(E)\,\mathrm{d}E}{\int \sigma(E)\,\mathrm{d}E}.$$

The integration limits are the energies of the beam at entrance and the exit of the target. The calculated energy averages were used as the input energies for the next iteration of the fit. The fit converges very fast. After five iterations, the calculated energies differ from the previous iteration by less than 0.1 MeV.

4. Conclusions

The setup described here is compact and portable. It is limited, though, in the beam intensities it can handle (less than 10^5 counts/s). This limit on beam intensity is dictated by the inability of the ionization chamber to handle higher rates and also by the need to keep the random background count rate down. The system is appropriate for measuring evaporation residue cross-sections down to a level of 1 mb. It can also provide useful data in cases where the beam is a mixture of nuclides.

We have shown how we can improve the signal to background ratio by using narrow time gates in our data reduction procedure. It is also possible to improve this system's performance by the application of narrow ADC time gates. Cross-section sensitivity can also be increased by using thicker targets but this has associated problems as outlined in the previous section. To study very low cross-sections ($\leqslant 100\,\mu$b) would require physically separating the beam from the reaction products. In some situations, reduction in the random background count rate could be achieved by introducing a small, precisely placed, beam stop made of heavy material in front of the ionization chamber window. This would result in lower efficiency for evaporation residue detection, but bring about a significant reduction in the random coincidence rates.

[1] It is noted that the form of this function is essentially the Wong formula [24]. Because the physics of the formula does not apply here, we do not call it the Wong formula in order not to confuse the readers. However, the functional form provides a good description of our data.

References

[1] M. Beckerman, et al., Phys. Rev. C 25 (1982) 837.
[2] R. Vandenbosch, Ann. Rev. Nucl. Part. Sci. 42 (1992) 447.
[3] M. Dasgupt, et al., Ann. Rev. Nucl. Part. Sci. 48 (1998) 401.
[4] P.H. Stelson, et al., Phys. Rev. C 41 (1990) 1584.
[5] H. Timmers, et al., Nucl. Phys. A 633 (1998) 421.
[6] F. Scarlassara, et al., Progr. Theoret. Phys. 154 (2004) 31.
[7] V.I. Zagrebaev, Phys. Rev. C 67 (2003) 061601 (R).
[8] D. Stracener, Nucl. Instr. and Meth. B 204 (2003) 42.
[9] D.J. Morrisey, Nucl. Instr. and Meth. B 204 (2003) 90.
[10] G. Munzenberg, Philos. Trans. Roy. Soc. London, Ser. A 356 (1998) 2083.
[11] Several presentations that discuss a variety of velocity separators, mass separators and other spectrometers suited for research with radioactive beams can be found at ⟨http://meetings.nscl.msu.edu/ria2004/talks.php⟩
[12] C.B. Fulmer, B.L. Cohen, Phys. Rev. 109 (1958) 94.
[13] M. Paul, et al., Nucl. Instr. and Meth. A 277 (1989) 418.
[14] J.F. Liang, et al., Nucl. Instr. and Meth. A 435 (1999) 393.
[15] W. Starzecki, A.M. Stefanini, S. Lunardix, C. Signorini, Nucl. Instr. and Meth. 193 (1982) 499.
[16] D. Shapira, T.A. Lewis, in: J.L. Duggan, I.L. Morgan (Eds.), Proceedings of the 17th Conference on Application of Accelerators in Research and Industry, AIP CP680, 2003, p. 545.
[17] D. Shapira, et al., Nucl. Instr. and Meth. A 449 (2000) 396.
[18] A. Gavron, Phys. Rev. C 21 (1999) 230.
[19] D. Shapira, et al., to be published.
[20] D. Shapira, et al., Nucl. Instr. and Meth. A 490 (2002) 159.
[21] J.F. Liang, et al., Phys. Rev. Lett. 91 (2003) 152701.
[22] J.F. Liang, et al., Progr. Theoret. Phys. 154 (2004) 106.
[23] W.S. Freeman, et al., Phys. Rev. Lett. 50 (1983) 1563.
[24] C.Y. Wong, Phys. Rev. Lett. 3 (1973) 766.